Early Disk-Galaxy Formation from JWST to the Milky Way
Proceedings IAU Symposium No. 377, 2024
F. Tabatabaei, B. Barbuy & Y.-S. Ting, eds.
doi:10.1017/S1743921323001102

Metal production in the early Universe: what chemical abundances in old stellar populations in the Milky Way tell us

Miho N. Ishigaki

National Astronomical Observatory of Japan, Mitaka, Tokyo 181-8588, Japan.
email: miho.ishigaki@nao.ac.jp

Abstract. Old stellar populations in our Galaxy provide fossil records of the metal enrichment in the first few billion years of the cosmic history. Growing elemental abundance data of individual stars combined with stellar ages and kinematics allow us to make constraints on characteristic properties of the metal-enrichment sources in the early Universe, such as the first stars. In order to interpret observed chemical abundances in the oldest stellar populations in terms of metal-enrichment sources, stellar and supernova yield models are crucial. In this article, we review how we can interpret observed chemical abundances in old stars in terms of the nature of metal enrichment sources. We discuss the limitations and the prospects of empirically constraining supernova yield models based on a large sample of extremely metal-poor stars. At the same time, we emphasize the importance of hunting old stars beyond the Solar neighborhood, which can be achieved with the next-generation multi-object spectrographs at large telescopes.

Keywords. The Milky Way Galaxy, Metal-poor stars, Chemical abundances

1. Overview

Metals constitute a tiny fraction of the universe today, but provide essential ingredients for stars, planets and life. Since nuclei of metals are created or destroyed only under extreme physical conditions, such as the core of stars or at the moment of supernova explosions, the observations of metals provide a useful probe of star formation over the cosmic time and at various galactic environment.

Metal production in the first few billion years from the Big Bang are of particular interest in many respects. First, metal enrichment sources in the early Universe can be very different from those of the present-day universe. The most obvious example is the first (Population III or Pop III) stars formed out of pristine hydrogen and helium gas, which were responsible for the first metal enrichment in the cosmic history (Abel *et al.* 2002; Hirano *et al.* 2014). Since the cooling of gas is inefficient under the metal-free environment, the gas clouds have to be extremely massive to gravitationally collapse to form stars. With this basic understanding, characteristic masses of Pop III stars are expected to well exceed 100s -1000s $M_{\odot}$ (Bromm & Larson 2004). Modern numerical simulations that are capable of resolving smaller scales with more complex physics have also found fragmentation to smaller masses and the formation of Pop III binaries or star clusters (see Klessen & Glover 2023, for a recent review). Knowing the nature of those first metal-enrichment sources are crucial to better understand not only their nucleosynthesis products but also a wide-range of phenomena that determine subsequent galaxy formation processes, e.g., the energies of ionizing photons, supernova feedback, the seeds of supermassive black hols, the formation of dust species (e.g., Jeon *et al.* 2014; Chiaki & Wise 2019; Toyouchi *et al.* 2023).

© The Author(s), 2024. Published by Cambridge University Press on behalf of International Astronomical Union.

https://doi.org/10.1017/S1743921323001102 Published online by Cambridge University Press

Second, the environment under which the metals are dispersed could be very different from the present-day universe. According to the hierarchical galaxy formation scenario predicted by the ΛCDM cosmological model, the first stars were formed under a shallow gravitational potential of a dark matter minihalo with $M \sin 10^6 M_\odot$ at redshifts of $> 10 - 20$ (Bromm & Larson 2004). Kinetic energies of supernovae could be comparable or larger than the gravitational binding energy of such a minihalo, which may end up with the escape of metals from the host halo. If the supernova explosion was extremely energetic, such as the case of pair-instability supernovae with explosion energy of $E \gtrsim 10^{52}$ erg, it destroys the host dark matter halo and prevent the prompt formation of the next generation stars (Whalen *et al.* 2008). Simulations predict that the mixing of ejected metals can be quite stochastic depending on various physical conditions in the early Universe (Ritter *et al.* 2015). Observational constraints on such a complex metal enrichment process in the early Universe are therefore desirable.

In this article, we discuss the production of metals in the early universe, with a particular focus on the implications from observed chemical abundances in old stellar populations in our Galaxy.

2. Extremely metal-poor stars as a fossil record of the first metal enrichment

The most promising fossil record of the first metal enrichment in the universe is extremely metal-poor (EMP) stars, which could be formed out of gas purely enriched by a few Pop III supernovae (Audouze & Silk 1995; Karlsson *et al.* 2013). Once a Pop III star is formed in a dark matter minihalo, metals are synthesized during the hydrostatic burning of the stellar evolution depending on the stellar masses (Heger & Woosley 2002). If the Pop III stars with masses greater than $\sim 10 M_\odot$, they could end up with a supernova explosion ejecting synthesized elements to interstellar medium. Numerical simulations suggest that the dilution of ejected metals with pristine hydrogen gas can result in the metallicity of the next generation stars up to about [Fe/H] ~ -2 to -3 (Ritter *et al.* 2012; Chiaki & Wise 2019). Under such a scenario, the observed elemental abundance ratios in EMP stars with [Fe/H] < -3 are likely preserving the elemental abundance patterns of the nucleosynthesis products of the progenitor Pop III star (Beers & Christlieb 2005; Frebel & Norris 2015).

2.1. *Growing observational data*

Although the EMP stars are extremely rare in the Solar neighborhood, thanks to wide-field surveys with high-resolution spectroscopic follow-up observations, we can now make use of statistical samples of detailed elemental abundances in these stars to infer their metal enrichment sources (The latest homogeneous analysis of 400 very metal-poor stars are presented in Aoki *et al.* 2022; Li *et al.* 2022). Figure 1 shows the elemental abundance ratios plotted against [Fe/H] from the compilation of various literature sources, thanks to all the past observational efforts (see Hartwig *et al.* 2023, and reference therein) as well as dedicated databases (e.g., Suda *et al.* 2008; Abohalima & Frebel 2018). Several key features can be noticed:

- Predominance of C-enhanced stars at the lowest metallicities. A subset of these stars show a remarkable similarity in their elemental abundance patterns (Aoki *et al.* 2018).
- large scatters in the abundance ratios of lighter elements, e.g., C/Fe or Mg/Fe. The Fe-peak elements show small scatters.

The question is whether the properties of individual Pop III supernovae can explain the observed scatters and correlations among different elemental abundances in EMP stars.

https://doi.org/10.1017/S1743921323001102 Published online by Cambridge University Press

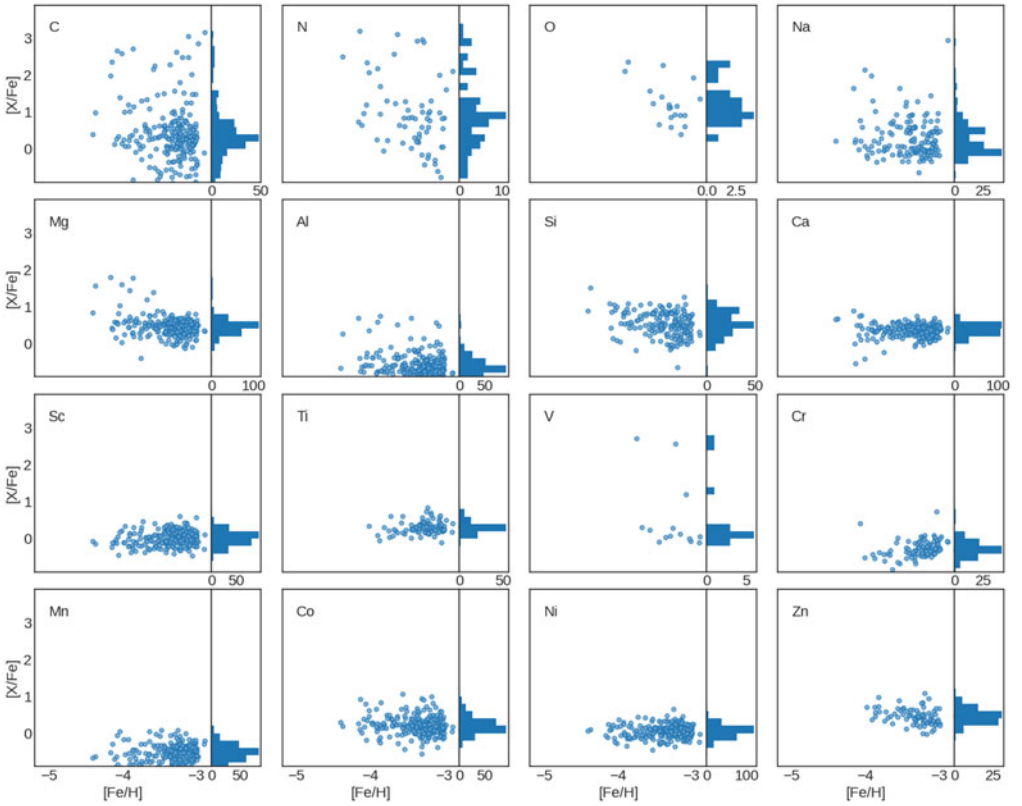

Figure 1. Observed elemental abundances in extremely metal-poor stars, compiled by Hartwig *et al.* (2023) from various literature sources.

2.2. *Supernova yield models of the first stars*

In principle, the production of metals in massive Pop III stars depend on the basic physical conditions such as the initial chemical composition, temperature, and density under which the nucleosynthesis occur (Heger & Woosley 2010; Limongi & Chieffi 2012; Nomoto *et al.* 2013). For example, carbon, nitrogen, oxygen are largely produced during the hydrostatic burning of stellar evolution and thus are more sensitive to progenitor stellar masses. On the other hand, Fe-peak elements are mostly produced during the supernova explosion, whose elemental yields depend on the maximum temperature experienced by the ejecta as the supernova shockwave passes through infalling stellar material. However, one of the largest factors that determines the final yields comes from the hydrodynamical properties of the ejecta, which are a subject of uncertainty from the astrophysical mechanism of supernova explosions. The simplest assumption is to employ a mass cut, which is the boundary in mass coordinate, above which the material is ejected to be incorporated to the next generation of stars. The material below that boundary falls back to form a compact remnant, such as a neutron star or a blackhole.

In reality, this is not a good approximation because of the mixing between the inner and outer layers of the progenitor Pop III star. If the explosion is close to spherically symmetric, the material close to the boundaries of different layers of elements are subject to Reighly-Taylor instability Joggerst *et al.* (2010). If the explosion is highly non-spherical, whose evidence has been commonly observed among local supernova remnants, the region of mixing can be more extensive Tominaga (2009).

https://doi.org/10.1017/S1743921323001102 Published online by Cambridge University Press

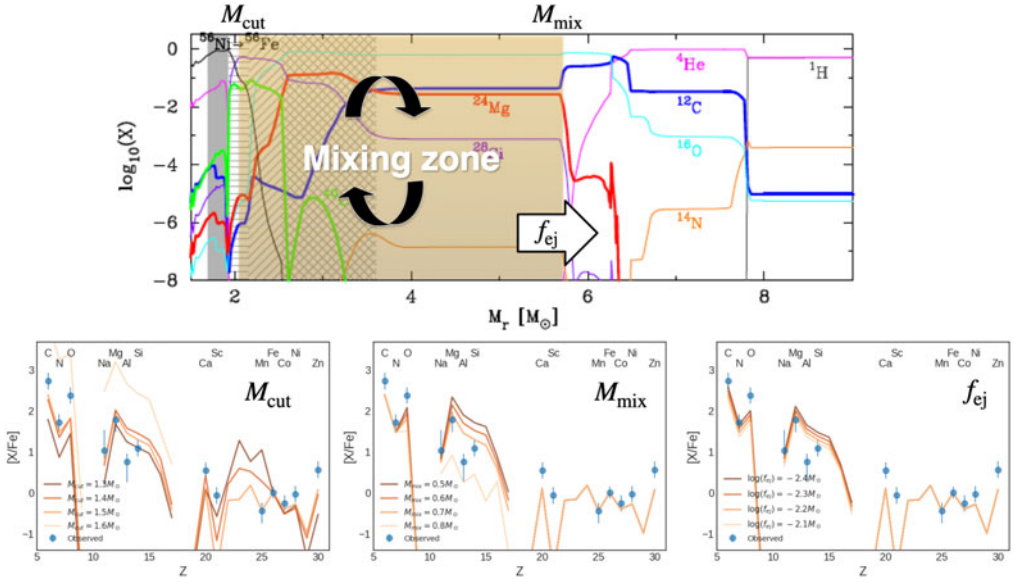

Figure 2. *Top*: Elemental abundance distribution after a supernova of $25M_\odot$ Pop III star. *Bottom*: Predicted abundance patterns varying the three parameters of the mixing-fallback model.

In order to calculate the Pop III supernova yields taking into account the effects of non-sphericity, multi-dimensional simulations are necessary. They are, however, highly computationally expensive and is challenging to explore a wide parameter range. As an alternative approach, the mixing-fallback model has been proposed as an analytic approximation to calculate the yields for such a non-spherical supernova (Umeda & Nomoto 2002; Tominaga *et al.* 2007). As illustrated in the top panel of Figure 2, the model employs three parameters, that correspond to (1) the inner boundary of the mixing zone close to the F-core: $M_{\rm cut}$, (2) the outer boundary of the mixing zone: $M_{\rm mix}$ and (3) the fraction of material in the mixing zone finally ejected: $f_{\rm ej}$. Despite of the simplicity, the yield model allows us to connect observed abundances to the nucleosynthesis sites in Pop III stars with very low computational costs, which allow for examining a wide parameter space to fit observations (Umeda & Nomoto 2002; Iwamoto *et al.* 2005; Tominaga *et al.* 2007, 2014). As we see in the following, this property may help identifying important parameters that explain the key features of observed abundance patterns and provide a benchmark for more realistic simulations (Chen *et al.* 2017).

To illustrate the dependence of the abundance patterns on the model parameters, the bottom panels of Figure 2 shows the observed abundance pattern of one of the sample stars compared with the predicted patterns for various mixing-fallback parameters (left, middle, and right panels for the $M_{\rm cut}$, $M_{\rm mix}$ and $f_{\rm ej}$ parameters, respectively). By varying $M_{\rm cut}$, we see a large variation in the abundances of Fe-peak elements, which are well constrained by the observed abundance. The middle panel shows the dependence of predicted yields on the $M_{\rm mix}$ parameter, scaled by the CO core mass. As expected, the abundance pattern of elements from Na to Si shows a large variation depending on this parameter. Finally, the right panel shows the predicted patterns by varying the ejected fraction, which change the ratio between elements that are loosely bound to the progenitor star like C or O and those that are tightly bound like Fe.

Thanks to a large sample of EMP stars, we could now obtain the Pop III progenitor masses and the range of parameters that are most compatible with the observed

https://doi.org/10.1017/S1743921323001102 Published online by Cambridge University Press

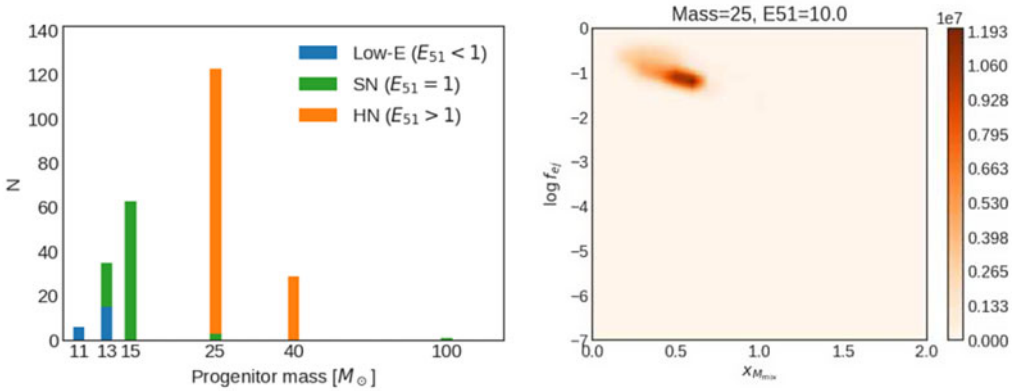

Figure 3. *Left*:The histogram of the progenitor masses of Pop III supernova yield models that best explain observed elemental abundances of EMP stars. *Right*: The combined likelihood for different combinations of $f_{\rm ej}$ and $M_{\rm mix}$ parameters. The vertical axis corresponds to the logarithm of $f_{\rm ej}$ parameter and the horizontal axis corresponds to the $M_{\rm mix}$ parameter scaled with the CO-core mass.

abundance distributions. The left panel of Figure 3 shows the histogram of the Pop III progenitor masses of our yield models that best fit each of the stellar abundance patterns of the latest compilation of EMP stars from Hartwig *et al.* (2023). The Pop III supernova model of $25M_\odot$ and explosion energy $E = 10 \times 10^{51}$ erg most frequently best explain the observed elemental abundances as seen in the earlier study of Ishigaki *et al.* (2018).

As we saw, observed elemental abundances also constrain the mixing-fallback parameters, which approximate the composition of supernova ejecta for an aspherical supernova. The right panel of Figure 3 shows the total likelihood in the log $f_{\rm ej}$ vs $M_{\rm mix}$ (scaled with the CO-core mass) plane for the Pop III model with a progenitor mass $M = 25M_\odot$ and $E_{51} = E/10^{51}{\rm erg} = 10$ model for the sample of EMP stars. This suggest that, under the current assumption of the yield models, $\sim 70\%$ of the material in the CO-core fallback, which would result in a black hole remnant of $\sim 5M_\odot$.

The approach mentioned above relies on individual Pop III stellar and supernova yields, which could be subject to large theoretical uncertainty. Among others, stellar rotation is predicted to have a large impact on Pop III stellar evolution and their yields (Yoon *et al.* 2012). Specifically, large changes in stellar yields as well as carbon/nitrogen elemental/isotopic ratios with rotational velocities are predicted as the result of stellar rotational mixing (Maeder & Meynet 2012; Choplin *et al.* 2019) Such rotating massive stars could be the progenitor of jetted supernovae (Grimmett *et al.* 2021) or hypernovae (Umeda & Nomoto 2005) which leave behind characteristic metal yields.

When comparing supernova yields with observed abundances of EMP stars, we should also keep in mind that the [Fe/H] of the observed star can be explained self consistently by the dilution of the ejected metals with pristine gas. Under the assumption of spherical symmetry and based on insights from hydrodynamical simulations, Magg *et al.* (2020) derived the minimum mass of pristine gas by which metals from a Pop III SN are diluted. This study highlights the importance of better understand the mechanism of metal mixing to extract information of Pop III stars from observed abundances in metal-poor stars.

We should also keep in mind the technical difficulty in observational side. For example, the chemical composition in the photosphere of an evolved star at present can be significantly different from the natal abundance of gas from which the star was formed as the result of convective mixing (Placco *et al.* 2014). The correction based on the stellar

https://doi.org/10.1017/S1743921323001102 Published online by Cambridge University Press

evolution model is needed to alleviate the bias caused by this effect. Furthermore, non-LTE or 3D effects could affect measured elemental abundances and need to be carefully corrected before extracting the inference on the Pop III stars (Norris & Yong 2019).

2.3. *More elaborated approach of interpreting the EMP observation with supernova yield models*

Now, one of the obvious shortcomings of the approach mentioned above is the assumption that only a single Pop III star contribute to the next generation of star (referred to "mono-enriched" scenario by Hartwig *et al.* 2019). Numerical simulations predict that Pop III stars are more likely formed as a star cluster, in which metals from multiple Pop III supernovae are together incorporated into the next generation of stars. If the majority of EMP stars were in fact enriched by multiple previous supernovae, the inference on the progenitor Pop III stars would be biased. Since the number of model parameters mentioned in the previous section would become too large to fit available observation, it seems impossible to constrain the parameter of the multi-enriched scenario. Hartwig *et al.* (2023) developed a novel approach of calculating the probability of multi enrichment using observed abundance ratios using a machine learning algorithm. Under the current set of yield models, it turned out that the majority is multi-enriched, while carbon-enhanced stars are more likely mono-enriched. This work opens the door for addressing the question of Pop III metal-enrichment beyond the standard assumption making the most of multi-element abundance measurements in upcoming surveys.

3. Old halo stars

3.1. *Other enrichment channels in the early Universe*

In the previous sections, we saw EMP stars are the promising fossil record of the metal enrichment in the early Universe. However, the EMP stars alone cannot address the metal-enrichment sources in the early Universe in general, because those EMP stars are expected to form only under the most pristine environment in the early Universe, where only a few SNe occur prior to their formation within a small DM halo. On the other hand, direct measurements of abundance ratios of high-Z objects such as damped Lyα absorption systems(Cooke *et al.* 2011), AGN/QSOs (Onoue *et al.* 2020; Yoshii *et al.* 2022), infer the Pop III nucleosynthesis may have occurred under diverse environment (e.g., Wells & Norman 2022). Also within the Milky Way, it has long been known that the oldest stellar populations, like those in globular clusters or the Galactic center, that the most ancient stars are not necessarily metal-poor (Barbuy *et al.* 2018). To have a complete picture of the diverse environment realized in the early phase of the Milky Way, an ideal way is to select stars by stellar ages, not with metallicity.

3.2. *Stellar Age-selected sample*

Is it possible to select stars that contain metals produced in the early Universe, without relying on [Fe/H]? In general, stellar age estimates are quite challenging (Soderblom 2010). Thanks to high-resolution spectroscopy in combination with Gaia astrometry, we have now access to precise stellar temperature, surface gravity and [Fe/H], which can be compared with stellar theoretical isochrone models to infer relative stellar ages (Sharma *et al.* 2018; Lindegren *et al.* 2020; Buder *et al.* 2021). Thanks to those high-resolution spectroscopic measurements by GALAH in combination with Gaia, Ishigaki *et al.* (2021) select main-sequence turn-off stars, whose position in the color-magnitude diagram is the most sensitive to stellar ages. From this sample, stars with

https://doi.org/10.1017/S1743921323001102 Published online by Cambridge University Press

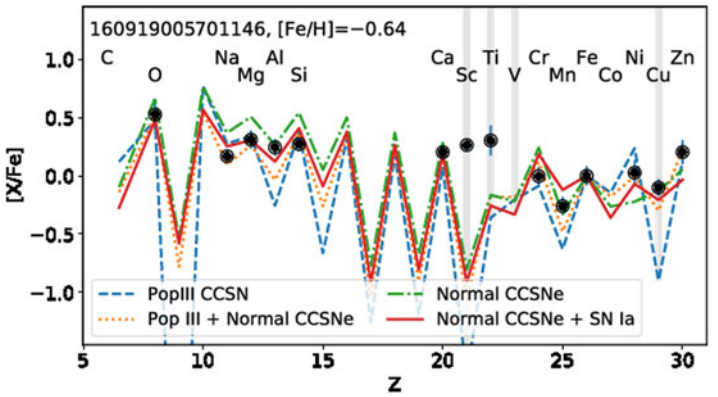

Figure 4. Predicted abundances of four different types of supernova yield models compared to the observed abundances of one of the sample star.

inferred stellar ages greater than 12 Gyrs and with halo-like kinematics are selected as the candidate of nearby old stars with detailed elemental abundances.

Figure 4 shows observed elemental abundances from GALAH compared with four different supernova yield models. By comparing the observed abundance patterns with different supernova yield models, Ishigaki *et al.* (2021) first examine weather the old halo stars contains metals synthesized by Pop III stars. As can be seen in Figure 4, the yields of Pop III core-collapse supernova (dashed-cyan line) generally show a stronger odd-even effect, which is not consistent with the observed elemental abundances in this specific star (black circles). The Pop III yield model with a small contamination from normal CCSNe (dotted-orange line) shows a better agreement with the observed elemental abundances. Those two scenarios, however, assume a Pop III SN to be the main contributor to the metals in the observed star. In this case, its [Fe/H] value should be almost realized by a single Pop III supernova event, which is not likely according to the theoretical prediction of hydrodynamical evolution of supernova ejecta (Magg *et al.* 2020). Indeed, cosmological simulation with semi-analytical models for the Pop III metal-enrichment suggests that, stars older than 12Gyrs and the [Fe/H] range of our sample, the expected fraction of Pop III metal enrichment is very small.

3.3. *Relative contribution of SNeIa to the nearby old stars*

A natural explanation of the observed elemental abundances of stars with [Fe/H]> -2 is the combination of IMF-averaged CCSNe and Type Ia supernovae (SNeIa). We parameterize an IMF slope of the CCSN progenitor, metallicity of CCSNe and the Fraction of SNeIa to calculate the yield models. Then for each star, we obtain the posterior probability distributions for the SNIa fraction given the observed elemental abundance pattern. The obtained fraction of SNIa is shown in the left panel of Figure 5. The three histograms for three subsets of characteristic abundances, high-alpha, low-alpha, and the metal-poor sub groups. The histograms show that the fraction of SNIa is up to 10 % of high-alpha sample and up to 20 % for the low-alpha group. These number fractions correspond to up to 44% of Fe in mass in the photosphere of the selected stars came from SNeIa (Ishigaki *et al.* 2021).

The masses of the progenitor white dwarf of SNeIa are currently unknown. Depending on the masses, whether the white dwarf has a mass either close to the Chandrasekhar mass ($M_{\rm Ch}$) or lower than $M_{\rm Ch}$ at the time of the explosion, resulting elemental yields are largely different (Leung & Nomoto 2018, 2020). To examine the contribution of

https://doi.org/10.1017/S1743921323001102 Published online by Cambridge University Press

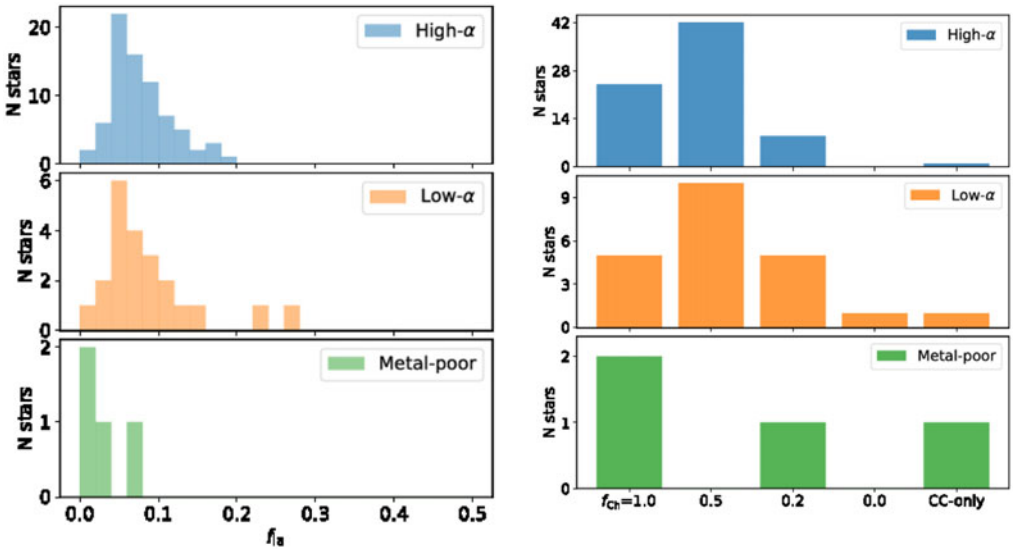

Figure 5. *Left*: Histograms of $f_{\rm Ia}$ obtained by fitting observed abundances from GALAH with the combined CCSNe+SN Ia yields. The top, middle and bottom panels show the results for the three groups defined by [Fe/H]-[Mg/Fe] diagram; High-α, Low-α and Metal-poor groups, respectively. *Right*: The number of stars that are best-fitted by the models with different assumptions about the SNeIa. The right-most bar corresponds to the CCSNe-only model without SNIa contribution. The four bars on the left correspond to the fraction of SNIa with near-Chandrasekhar mass WD progenitor of 1.0, 0.5, 0.2, and 0.0, respectively.

metals from these two types of SNIa yield models, for each observed star, we obtain a ranking of the quality of the fit for five different relative fraction of near-$M_{\rm Ch}$ SNIa by penalizing with the number of parameters. The right panel of Figure 5 shows the histograms summarizing a top-ranking model for all of the stars. The right most bar corresponds to the CCNS only model, while the four bars on the left correspond to the combined CCSNe + SN Ia with various near-$M_{\rm Ch}$ SNeIa fractions (1.0, 0.5, 0.3, and 0.0, from the left to right). Overall, the majority of low and high-alpha group stars are best explained by the models with some contribution from sub-$M_{\rm Ch}$ SNeIa. Whether or not this channel for SNIa progenitors are dominant should be investigated with a wider range of SNIa yield models.

4. Toward complete characterization of chemical diversity in old stellar populations

So far, we have discussed the implications on the early metal-enrichment sources from old stellar populations in the Solar neighborhood, either selected by [Fe/H] or by relative ages. On the other hand, signatures of more pristine or diverse chemical abundances in the Milky Way halo beyond $\sim$10 kpc have begun to emerge and their connection to the Milky Way's accretion history have been a subject of discussion (Fernández-Alvar *et al.* 2017; Naidu *et al.* 2020).

Although various uncertainties in theoretical supernova yield models currently remain, we showed prospects to observationaly constrain these yield models with elemental abundances of much larger samples than currently available, thanks to on-going and planned multi-object spectroscopic surveys, such as WEAVE, Milky Way Mapper, 4MOST, or DESI. Among others, the Prime Focus Spectrograph (PFS) on the Subaru Telescope (Takada *et al.* 2014) is uniquely capable of spectroscopic metallicity and velocity estimate at the outer reaches of the Milky Way (outer disk/halo). With those upcoming

https://doi.org/10.1017/S1743921323001102 Published online by Cambridge University Press

surveys probing old stellar populations formed under various environments, we will be able to capture the true diversity in metal-enrichment sources in the early Universe.

MNI is supported by JSPS KAKENHI Grant Numbers JP17K14249, JP18H05437, JP20H05855, JP21H04499.

References

Abel, T., Bryan, G. L., & Norman, M. L. 2002, Science, 295, 93
Abohalima, A., & Frebel, A. 2018, ApJS, 238, 36
Aoki, W., Matsuno, T., Honda, S., *et al.* 2018, PASJ, 70, 94
Aoki, W., Li, H., Matsuno, T., *et al.* 2022, ApJ, 931, 146
Audouze, J., & Silk, J. 1995, ApJ, 451L, 49
Barbuy B., Chiappini C., Gerhard O. 2018, ARA&A, 56, 223
Beers, T. C., & Christlieb, N. 2005, ARA&A, 43, 531
Bessell, M. S., Collet, R., Keller, S. C., *et al.* 2015, ApJ, 806, 16
Bromm, V., & Larson, R. B. 2004, ARA&A, 42, 79
Bromm, V., & Yoshida, N. 2011, ARA&A, 49, 373
Buder S. *et al.* 2021, MNRAS, 506, 150
Chen, K.-J., Heger, A., Whalen, D. J., *et al.* 2017, MNRAS, 467, 4731
Chiaki, G., & Wise, J. H. 2019, MNRAS, 482, 3933
Choplin, A., Tominaga, N., & Ishigaki, M. N. 2019, A&A, 632, A62
Cooke, R., Pettini, M., Steidel, C. C., Rudie, G. C., & Nissen, P. E. 2011, MNRAS, 417, 1534
Fernández-Alvar, E., Carigi, L., Allende Prieto, C., *et al.* 2017, MNRAS, 465, 1586
Frebel, A., & Norris, J. E. 2015, ARA&A, 53, 631
Grimmett, J. J., Müller B., Heger, A., Banerjee, P.,& Obergaulinger, M. 2021, MNRAS, 501, 2764
Hartwig, T., Ishigaki, M. N., Klessen, R. S., & Yoshida, N. 2018, MNRAS, 482, 1204
Hartwig, T., Ishgiaki, M. I., Kobayashi, C., Tominaga, N. 2023, ApJ in press
Heger, A., & Woosley, S. E. 2002, ApJ, 567, 532
Heger A., & Woosley S. E. 2010, ApJ, 724, 341
Hirano, S., Hosokawa, T., Yoshida, N., *et al.* 2014, ApJ, 781, 60
Ishigaki, M. N., Tominaga, N., Kobayashi, C., & Nomoto, K. 2018, ApJ, 857, 46
Ishigaki, M. N., Hartwig, T., Tarumi, Y., *et al.* 2021, MNRAS, 506, 5410
Iwamoto, N., Umeda, H., Tominaga, N., Nomoto, K., & Maeda, K. 2005, Science, 309, 451
Jeon, M., Pawlik, A. H., Bromm, V., & Milosavljević, M. 2014, MNRAS, 444, 3288
Joggerst, C. C., Almgren, A., & Woosley, S. E. 2010, ApJ, 723, 353
Karlsson, T., Bromm, V., & Bland-Hawthorn, J. 2013, RvMP, 85, 809
Keller, S. C., Bessell, M. S., Frebel, A., *et al.* 2014, Nature, 506, 463
Klessen, R. S., Glover, S. C. O. 2023, arXiv:2303.12500
Leung, S.-C., & Nomoto, K. 2018, ApJ, 861, 143
Leung, S.-C., & Nomoto, K. 2020, ApJ, 888, 80
Li, H., Aoki, W., Matsuno, T., *et al.* 2022, ApJ, 931, 147
Limongi, M., & Chieffi, A. 2012, ApJS, 199, 38
Lindegren L. *et al.* 2020, A&A, 649, 35
Maeder, A., & Meynet, G. 2012, RvMP, 84, 25
Magg, M., Nordlander, T., Glover, S. C. O., *et al.* 2020, MNRAS, 498, 3703
Naidu, R. P., Conroy, C., Bonaca, A., *et al.* 2020, ApJ, 901, 48
Nomoto, K., Kobayashi, C., Tominaga, N. 2013, ARA&A, 51, 457
Norris, J. E., & Yong, D. 2019, ApJ, 879, 37
Onoue, M., Bañados, E., Mazzucchelli, C. *et al.* 2020, ApJ, 898, 105
Placco, V. M., Frebel, A., Beers, T. C., & Stancliffe, R. J. 2014, ApJ, 797, 21
Ritter, J. S., Safranek-Shrader, C., Gnat, O., Milosavljević, M., & Bromm, V. 2012, ApJ, 761, 56
Ritter, J. S., Sluder, A., Safranek-Shrader, C., Milosavljević, M., & Bromm, V. 2015, MNRAS, 451, 1190

https://doi.org/10.1017/S1743921323001102 Published online by Cambridge University Press

Sharma, S. *et al.* 2018, MNRAS, 473, 2004
Soderblom D. R. 2010, ARA&A, 48, 581
Suda, T., Katsuta, Y., Yamada, S., *et al.* 2008, PASJ, 60, 1159
Takada, M., *et al.* 2014, PASJ, 66, R1
Tominaga, N., Umeda, H., Nomoto, K. 2007, ApJ, 660, 516
Tominaga, N. 2009, ApJ, 690, 526
Tominaga, N., Iwamoto, N., & Nomoto, K. 2014, ApJ, 785, 98
Toyouchi, D., Inayoshi, K., Ishigaki, M. N., & Tominaga, N. 2022, MNRAS, 512, 2573
Toyouchi, D., Inayoshi, K., Li, W., Haiman, Z., & Kuiper, R. 2023, MNRAS, 518, 1601
Umeda, H., & Nomoto, K. 2002, ApJ, 565, 385
Umeda, H., & Nomoto, K. 2005, ApJ, 619, 427
Whalen, D., van Veelen, B., O'Shea, B. W., & Norman, M. L. 2008, ApJ, 682, 49
Wells, A. I., & Norman, M. L. 2022, ApJ, 932, 71
Yoon S. C., Dierks, A., Langer, N. 2012, A&A, 542, A113
Yoshii, Y., Sameshima, H., Tsujimoto, T. 2022, ApJ, 937, 61

https://doi.org/10.1017/S1743921323001102 Published online by Cambridge University Press